

Parallel tempering on optimized paths

Saifuddin Syed^{*1} Vittorio Romaniello^{*1} Trevor Campbell¹ Alexandre Bouchard-Côté¹

Abstract

Parallel tempering (PT) is a class of Markov chain Monte Carlo algorithms that constructs a path of distributions annealing between a tractable reference and an intractable target, and then interchanges states along the path to improve mixing in the target. The performance of PT depends on how quickly a sample from the reference distribution makes its way to the target, which in turn depends on the particular path of annealing distributions. However, past work on PT has used only simple paths constructed from convex combinations of the reference and target log-densities. This paper begins by demonstrating that this path performs poorly in the setting where the reference and target are nearly mutually singular. To address this issue, we expand the framework of PT to general families of paths, formulate the choice of path as an optimization problem that admits tractable gradient estimates, and propose a flexible new family of spline interpolation paths for use in practice. Theoretical and empirical results both demonstrate that our proposed methodology breaks previously-established upper performance limits for traditional paths.

1. Introduction

Markov Chain Monte Carlo (MCMC) methods are widely used to approximate intractable expectations with respect to un-normalized probability distributions over general state spaces. For hard problems, MCMC can suffer from poor mixing. For example, faced with well-separated modes, MCMC methods often get trapped exploring local regions of high probability. Parallel tempering (PT) is a widely applicable methodology (Geyer, 1991) to tackle poor mixing of MCMC algorithms.

Suppose we seek to approximate an expectation with respect

to an intractable *target distribution* π_1 . Denote by π_0 a *reference distribution* defined on the same space, which is assumed to be tractable in the sense of the availability of an efficient sampler. This work is motivated by the case where π_0 and π_1 are nearly mutually singular. A typical case is where the target is a Bayesian posterior distribution, the reference is the prior—for which i.i.d. sampling is typically possible—and the prior is misspecified.

PT methods are based on a specific continuum of distributions $\pi_t \propto \pi_0^{1-t} \pi_1^t$, $t \in [0, 1]$, bridging π_0 and π_1 . This path of intermediate distributions is known as the power posterior path in the literature, but in our framework it will be more natural to think of these continua as a *linear paths*, as they linearly interpolate between log-densities. PT algorithms discretize the path at some $0 = t_0 < \dots < t_N = 1$ to obtain a sequence of distributions $\pi_{t_0}, \pi_{t_1}, \dots, \pi_{t_N}$. See Figure 1 (top) for an example of a linear path for two nearly mutually singular Gaussian distributions.

Given the path discretization, PT involves running $N + 1$ MCMC chains that together target the product distribution $\pi_{t_0} \pi_{t_1} \dots \pi_{t_N}$. Based on the assumption that the chain π_0 can be sampled efficiently, PT uses swap-based interactions between neighbouring chains to propagate the exploration done in π_0 into improved exploration in the chain of interest π_1 . By designing these swaps as Metropolis–Hastings moves, PT guarantees that the marginal distribution of the N^{th} chain converges to π_1 ; and in practice, the rate of convergence is often much faster compared to running a single chain (Woodard et al., 2009). PT algorithms are extensively used in hard sampling problems arising in statistics, physics, computational chemistry, phylogenetics, and machine learning (Desjardins et al., 2014; Ballnus et al., 2017; Kamberaj, 2020; Müller & Bouckaert, 2020).

Notwithstanding empirical and theoretical successes, existing PT algorithms also have well-understood theoretical limitations. Earlier work focusing on the theoretical analysis of reversible variants of PT has shown that adding too many intermediate chains can actually deteriorate performance (Lingenheil et al., 2009; Atchadé et al., 2011). Recent work (Syed et al., 2019) has shown that a nonreversible variant of PT (Okabe et al., 2001) is guaranteed to dominate its classical reversible counterpart, and moreover that in the nonreversible regime adding more chains is guaranteed to

^{*}Equal contribution ¹Department of Statistics, University of British Columbia, Vancouver, Canada. Correspondence to: Saifuddin Syed <saif.syed@stat.ubc.ca>, Vittorio Romaniello <vittorio.romaniello@stat.ubc.ca>.

improve performance. However, even with these more efficient non reversible PT algorithms, Syed et al. (2019) established that the improvement brought by higher parallelism will asymptote to a fundamental limit known as the *global communication barrier*.

In this work, we show that by generalizing the class of paths interpolating between π_0 and π_1 from linear to nonlinear, the global communication barrier can be broken, leading to substantial performance improvements. Importantly, the nonlinear path used to demonstrate this breakage is computed using a practical algorithm that can be used in any situation where PT is applicable. An example of a path optimized using our algorithm is shown in Figure 1 (bottom).

We also present a detailed theoretical analysis of parallel tempering algorithms based on nonlinear paths. Using this analysis we prove that the performance gains obtained by going from linear to nonlinear path PT algorithms can be arbitrarily large. Our theoretical analysis also motivates a principled objective function used to optimize over a parametric family of paths.

Literature review Beyond parallel tempering, several methods to approximate intractable integrals rely on a path of distributions from a reference to a target distribution, and there is a rich literature on the construction and optimization of nonlinear paths for annealed importance sampling type algorithms (Gelman & Meng, 1998; Rischard et al., 2018; Grosse et al., 2013; Brekelmans et al., 2020). These algorithms are highly parallel; however, for challenging problems, even when combined with adaptive step size procedures (Zhou et al., 2016) they typically suffer from particle degeneracy (Syed et al., 2019, Sec. 7.4). Moreover, these methods use different path optimization criteria which are not well motivated in the context of parallel tempering. The most closely related work is Tawn et al. (2020), which considers a specific example of a nonlinear path, distinct from the one considered here. Moreover the construction of the nonlinear path in this previous work requires knowledge of the location of modes of π_1 and hence makes the overall algorithm much less broadly applicable than standard PT.

2. Background

In this section, we provide a brief overview of parallel tempering (PT) (Geyer, 1991), as well as recent results on nonreversible communication (Okabe et al., 2001; Sakai & Hukushima, 2016; Syed et al., 2019). Define a reference unnormalized density function π_0 for which sampling is tractable, and an unnormalized target density function π_1 for which sampling is intractable; the goal is to obtain samples from π_1 .¹ Define a path of distributions $\pi_t \propto \pi_0^{1-t} \pi_1^t$

¹We assume all distributions share a common state space \mathcal{X} throughout, and will often suppress the arguments of (log-)density

for $t \in [0, 1]$ from the reference to the target. Finally, define the annealing schedule \mathcal{T}_N to be a monotone sequence in $[0, 1]$, satisfying

$$\mathcal{T}_N = (t_n)_{n=0}^N, \quad 0 = t_0 \leq t_1 \leq \dots \leq t_N = 1$$

$$\|\mathcal{T}_N\| = \max_{n \in \{0, \dots, N-1\}} t_{n+1} - t_n.$$

The core idea of parallel tempering is to construct a Markov chain (X_m^0, \dots, X_m^N) , $m = 1, 2, \dots$ that (1) has invariant distribution $\pi_{t_0} \cdot \pi_{t_1} \cdots \pi_{t_N}$ —such that we can treat the marginal chain X_n^N as samples from the target π_1 —and (2) swaps components of the state vector such that independent samples from component 0 (i.e., the reference π_0) traverse along the annealing path and aid mixing in component N (i.e., the target π_1). This is possible to achieve by iteratively performing a *local exploration* move followed by a *communication* move as shown in Algorithm 1.

Local Exploration Given $(X_{m-1}^0, \dots, X_{m-1}^N)$, we obtain an intermediate state $(\tilde{X}_m^0, \dots, \tilde{X}_m^N)$ by updating the n^{th} component using any MCMC move targeting π_{t_n} , for $n = 0, \dots, N$. This move can be performed in parallel across components since each is updated independently.

Communication Given the intermediate state $(\tilde{X}_m^0, \dots, \tilde{X}_m^N)$, we apply pairwise swaps of components n and $n + 1$, $n \in S_m \subset \{0, \dots, N - 1\}$ for swapped index set S_m . Formally, a swap is a move from (x^0, \dots, x^N) to $(x^0, \dots, x^{n+1}, x^n, \dots, x^N)$, which is accepted with probability

$$\alpha_n = 1 \wedge \frac{\pi_{t_n}(x^{n+1})\pi_{t_{n+1}}(x^n)}{\pi_{t_n}(x^n)\pi_{t_{n+1}}(x^{n+1})}. \quad (1)$$

Since each swap only depends on components $n, n + 1$, one can perform all of the swaps in S_m in parallel, as long as $n \in S_m$ implies $(n + 1) \notin S_m$. The largest collection of such non-interfering swaps is $S_m \in \{S_{\text{even}}, S_{\text{odd}}\}$, where $S_{\text{even}}, S_{\text{odd}}$ are the even and odd subsets of $\{0, \dots, N - 1\}$ respectively. In *non-reversible PT* (NRPT) (Okabe et al., 2001), the swap set S_m at each step m is set to

$$S_m = \begin{cases} S_{\text{even}} & m \text{ even} \\ S_{\text{odd}} & m \text{ odd.} \end{cases}$$

Based on simplifying assumptions on the local exploration moves, recent work has shown that if $r(t, t')$ is the probability of a swap being rejected between chains at t, t' , then the *round trip rate* $\tau(\mathcal{T}_N)$ —the frequency at which a new sample from the reference π_0 percolates to the target π_1 and then back to π_0 —is (Syed et al., 2019, Cors. 1,2),

$$\tau(\mathcal{T}_N) = \left(2 + 2 \sum_{n=0}^{N-1} \frac{r(t_n, t_{n+1})}{1 - r(t_n, t_{n+1})} \right)^{-1}. \quad (2)$$

functions—i.e., π_1 instead of $\pi_1(x)$ —for notational brevity.

Algorithm 1 NRPT

Require: state \mathbf{x}_0 , path π_t , schedule \mathcal{T}_N , # iterations M

$r_n \leftarrow 0$ for all $n \in \{0, \dots, N-1\}$

for $m = 1$ **to** M **do**

$\tilde{\mathbf{x}}_m \leftarrow \text{LocalExploration}(\mathbf{x}_{m-1})$

$S_m \leftarrow S_{\text{even}}$ if m is even, otherwise $S_m \leftarrow S_{\text{odd}}$

for $n = 0$ **to** $N-1$ **do**

$\alpha_n \leftarrow 1 \wedge \frac{\pi_{t_n}(x^{n+1})\pi_{t_{n+1}}(x^n)}{\pi_{t_n}(x^n)\pi_{t_{n+1}}(x^{n+1})}$

$r_n \leftarrow r_n + (1 - \alpha_n)$

$U_n \sim \text{Unif}(0, 1)$

if $n \in S_m$ **and** $U_n \leq \alpha_n$ **then**

$(\tilde{x}_m^n, \tilde{x}_m^{n+1}) \leftarrow (\tilde{x}_m^{n+1}, \tilde{x}_m^n)$

end if

$\mathbf{x}_m \leftarrow \tilde{\mathbf{x}}_m$

end for

end for

$r_n \leftarrow r_n/M$ for $n \in \{0, \dots, N-1\}$

Return: $\{\mathbf{x}_m\}_{m=1}^M, \{r_n\}_{n=0}^{N-1}$

Further, if \mathcal{T}_N is refined so that $\|\mathcal{T}_N\| \rightarrow 0$ as $N \rightarrow \infty$, we find that the asymptotic (in N) round trip rate is

$$\tau_\infty = \lim_{N \rightarrow \infty} \tau(\mathcal{T}_N) = (2 + 2\Lambda)^{-1}, \quad (3)$$

where $\Lambda \geq 0$ is a constant associated with the pair π_0, π_1 called the *global communication barrier* (Syed et al., 2019). Note that Λ does not depend on the number of chains N or discretization schedule \mathcal{T}_N .

3. General annealing paths

In the following, we use the terminology *annealing path* to describe a continuum of distributions interpolating between π_0 and π_1 ; this definition will be formalized shortly. The previous work reviewed in the last section assumes that the annealing path has the form $\pi_t \propto \pi_0^{1-t} \pi_1^t$, i.e., that the annealing path linearly interpolates between the log densities. A natural question is whether using other paths could lead to an improved round trip rate.

In this work we show that the answer to this question is positive: the following proposition demonstrates that the traditional path $\pi_t \propto \pi_0^{1-t} \pi_1^t$ suffers from an arbitrarily suboptimal global communication barrier even in simple examples with Gaussian reference and target distributions.

Proposition 1. *Suppose the reference and target distributions are $\pi_0 = \mathcal{N}(\mu_0, \sigma^2)$ and $\pi_1 = \mathcal{N}(\mu_1, \sigma^2)$, and define $z = |\mu_1 - \mu_0|/\sigma$. Then as $z \rightarrow \infty$,*

1. *the path $\pi_t \propto \pi_0^{1-t} \pi_1^t$ has $\tau_\infty = \Theta(1/z)$, and*
2. *there exists a path of Gaussians distributions with $\tau_\infty = \Omega(1/\log z)$.*

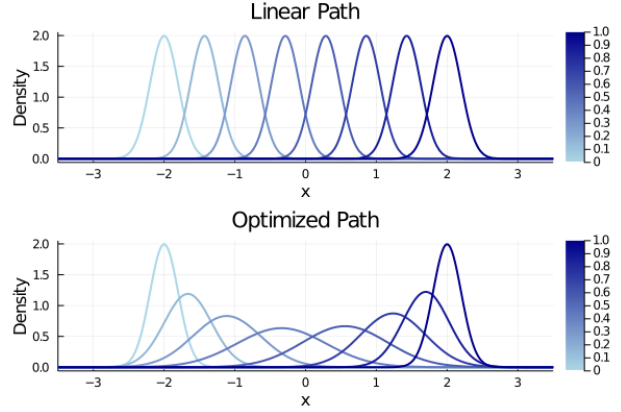


Figure 1. Two annealing paths between a $\pi_0 = \mathcal{N}(-2, 0.2^2)$ (light blue) and $\pi_1 = \mathcal{N}(2, 0.2^2)$ (dark blue): the traditional linear path (top) and an optimized nonlinear path (bottom). While the distributions in the linear path are nearly mutually singular, the optimized path overlap substantially, leading to faster round trips.

Therefore, upon decreasing the variance of the reference and target while holding their means fixed, the traditional linear annealing path obtains an exponentially smaller asymptotic round trip rate than the optimal path of Gaussians. Figure 1 provides an intuitive explanation. The standard path (top) corresponds to a set of Gaussian distributions with mean interpolated between the reference and target. If one reduces the variance of the reference and target, so does the variance of the distributions along the path. For any fixed N , these distributions become nearly mutually singular, leading to arbitrarily low round trip rates. The solution to this issue (bottom) is to allow the distributions along the path to have increased variances, thereby maintaining mutual overlap and the ability to swap components with a reasonable probability. This motivates the need to design more general annealing paths. In the following, we introduce the precise general definition of an annealing path, an analysis of path communication efficiency in parallel tempering, and a rigorous formulation of—and solution to—the problem of tuning path parameters to maximize communication efficiency.

3.1. Assumptions

Let $\mathcal{P}(\mathcal{X})$ be the set of probability densities with full support on a state space \mathcal{X} . For any collection of densities $\pi_t \in \mathcal{P}(\mathcal{X})$ with index $t \in [0, 1]$, associate to each a log-density function W_t such that

$$\pi_t(x) = \frac{1}{Z_t} \exp(W_t(x)), \quad x \in \mathcal{X}, \quad (4)$$

where $Z_t = \int_{\mathcal{X}} \exp(W_t(x)) dx$ is the normalizing constant. Definition 1 provides the conditions necessary to form a path of distributions from a reference π_0 to a target π_1 that

are well-behaved for use in parallel tempering.

Definition 1. An annealing path for a target density π is a map $[0, 1] \rightarrow \mathcal{P}(\mathcal{X})$, denoted $t \mapsto \pi_t$, such that:

1. the right endpoint is the target distribution $\pi_1 = \pi$,
2. for each $x \in \mathcal{X}$, the log density $W_t(x) : [0, 1] \rightarrow \mathbb{R}$ is piecewise twice continuously differentiable in t , and
3. there exist $V_1, V_2 : \mathcal{X} \rightarrow [0, \infty)$ such that for all $x \in \mathcal{X}$ and all $t \in [0, 1]$ with defined derivatives,

$$\left| \frac{dW_t}{dt}(x) \right| \leq V_1(x), \quad \left| \frac{d^2W_t}{dt^2}(x) \right| \leq V_2(x),$$

and

$$\sup_{t \in [0, 1]} \mathbb{E}_{\pi_t}[V_1^3 + V_2] < \infty.$$

There are many ways to move beyond the standard linear path $\pi_t \propto \pi_0^{1-t} \pi_1^t$. For example, consider a nonlinear path $\pi_t \propto \pi_0^{\eta_0(t)} \pi_1^{\eta_1(t)}$ where $\eta_i : [0, 1] \rightarrow \mathbb{R}$ are functions such that $\eta_0(0) = \eta_1(1) = 1$ and $\eta_0(1) = \eta_1(0) = 0$. An example of such functions is the cubic Bézier curve

$$\begin{aligned} \eta_0(t) &= (1-t)((1-t)^2 + 3(1-t)t + 3t^2) \\ \eta_1(t) &= t(3(1-t)^2 + 3(1-t)t + t^2). \end{aligned}$$

As long as for all $t \in [0, 1]$, π_t is a normalizable density and the appropriate moment bounds exist per Definition 1, this is a valid annealing path. Further, note that the path parameter does not necessarily have to appear as an exponent: consider for example the mixture path $\pi_t \propto (1-t)\pi_0 + t\pi$. Section 4 provides a more detailed example based on linear splines.

3.2. Communication efficiency analysis

Given a particular annealing path satisfying Definition 1, we require a method to characterize the round trip rate performance of parallel tempering based on that path. The results presented in this section form the basis of the objective function used to optimize over paths, as well as the foundation for the proof of Proposition 1.

We start with some notation for the rejection rates involved when Algorithm 1 is used with nonlinear paths (Equation 4). For $t, t' \in [0, 1]$, $x \in \mathcal{X}$, define the rejection rate function $r : [0, 1]^2 \rightarrow [0, 1]$ to be

$$\begin{aligned} r(t, t') &= 1 - \mathbb{E}[\exp(\min\{0, A_{t,t'}(X, X')\})] \\ A_{t,t'}(x, x') &= (W_{t'}(x) - W_t(x)) - (W_{t'}(x') - W_t(x')), \end{aligned}$$

where $X \sim \pi_t$ and $X' \sim \pi_{t'}$ are independent. Assuming that all chains have reached stationarity, and all chains undergo *efficient local exploration*—i.e., $W_t(X), W_t(\tilde{X})$ are independent when $X \sim \pi_t$ and \tilde{X} is generated by local

exploration from X —then the round trip rate for a particular schedule \mathcal{T}_N has the form given earlier in Equation (2). This statement follows from (Syed et al., 2019, Cor. 1) without modification, because the proof of that result does not depend on the form of the acceptance ratio.

Our next objective is to characterize the asymptotic communication efficiency of a nonlinear path in the regime where $N \rightarrow \infty$ and $\|\mathcal{T}_N\| \rightarrow 0$ —which establishes its fundamental ability to take advantage of parallel computation. In other words, we require a generalization of the asymptotic result in Equation (3). In this case, previous theory relies on the particular form of the acceptance ratio for linear paths (Syed et al., 2019); in the remainder of this section, we provide a generalization of the asymptotic result for nonlinear paths by piecewise approximation by a linear spline.

For $t, t' \in [0, 1]$, define $\Lambda(t, t')$ to be the global communication barrier for the linear secant connecting π_t and $\pi_{t'}$,

$$\begin{aligned} \Lambda(t, t') &= \frac{1}{2} \int_0^1 \mathbb{E}[|A_{t,t'}(X_s, X'_s)|] ds, \\ X_s, X'_s &\stackrel{\text{i.i.d.}}{\sim} \frac{1}{Z^{t,t'}(s)} \exp((1-s)W_t + sW_{t'}). \end{aligned} \quad (5)$$

Lemma 1 shows that the global communication barrier $\Lambda(t, t')$ along the secant of the path connecting t to t' is a good approximation of the true rejection rate $r(t, t')$ with $O(|t - t'|^3)$ error as $t \rightarrow t'$.

Lemma 1. For any annealing path, there exists a constant $C < \infty$ independent of t, t' such that for all $t, t' \in [0, 1]$,

$$|r(t, t') - \Lambda(t, t')| \leq C|t - t'|^3. \quad (6)$$

A direct consequence of Lemma 1 is that for any fixed schedule \mathcal{T}_N ,

$$\left| \sum_{n=0}^{N-1} r(t_n, t_{n+1}) - \Lambda(\mathcal{T}_N) \right| \leq C\|\mathcal{T}_N\|^2, \quad (7)$$

where $\Lambda(\mathcal{T}_N) = \sum_{n=0}^{N-1} \Lambda(t_n, t_{n+1})$. Intuitively, in the $\|\mathcal{T}_N\| \approx 0$ regime where rejection rates are low,

$$\frac{r(t_n, t_{n+1})}{1 - r(t_n, t_{n+1})} \approx r(t_n, t_{n+1}),$$

and we have that $\tau(\mathcal{T}_N) \approx (2 + 2\Lambda(\mathcal{T}_N))^{-1}$. Therefore, $\Lambda(\mathcal{T}_N)$ characterizes the communication efficiency of the path in a way that naturally extends the global communication barrier from the linear path case. Theorem 2 provides the precise statement: the convergence is uniform in \mathcal{T}_N and depends only on $\|\mathcal{T}_N\|$, and $\Lambda(\mathcal{T}_N)$ itself converges to a constant Λ in the asymptotic regime. We refer to Λ , defined below in Equation (9) as the global communication barrier for the general annealing path.

Theorem 2. *If there exists an $\epsilon > 0$ such that*

$$\sup_{t \in [0,1]} \mathbb{E}_{\pi_t} [(1 + V_1) \exp(\epsilon V_2)] < \infty,$$

then

$$\lim_{\epsilon \rightarrow 0} \sup_{\mathcal{T}_N: \|\mathcal{T}_N\| \leq \epsilon} |(2 + 2\Lambda(\mathcal{T}_N))^{-1} - \tau(\mathcal{T}_N)| = 0 \quad (8)$$

$$\text{and } \lim_{\epsilon \rightarrow 0} \sup_{\mathcal{T}_N: \|\mathcal{T}_N\| \leq \epsilon} |\Lambda(\mathcal{T}_N) - \Lambda| = 0, \quad (9)$$

where $\Lambda = \int_0^1 \lambda(t) dt$ for an instantaneous rejection rate function $\lambda : [0, 1] \rightarrow [0, \infty)$ given by

$$\begin{aligned} \lambda(t) &= \lim_{\Delta t \rightarrow 0} \frac{r(t + \Delta t, t)}{|\Delta t|} \\ &= \frac{1}{2} \mathbb{E} \left[\left| \frac{dW_t}{dt}(X_t) - \frac{dW_t}{dt}(X'_t) \right| \right], \quad X_t, X'_t \stackrel{i.i.d.}{\sim} \pi_t. \end{aligned}$$

The integrability condition is required to control the tail behaviour of distributions formed by linearized approximations to the path π_t . This condition is satisfied by a wide range of annealing paths, e.g., the linear spline paths proposed in this work in Section 4—since in that case $V_2 = 0$.

3.3. Annealing path families and optimization

It is often the case that there are a set of candidate annealing paths in consideration for a particular target π . For example, if a path has tunable parameters $\phi \in \Phi$ that govern its shape, we can generate a collection of annealing paths that all target π by varying the parameter ϕ . We call such collections an annealing path family.

Definition 3. *An annealing path family for π is a set of annealing paths π_t that target π .*

There are many ways to construct useful annealing path families. For example, if one is provided a parametric family of variational distributions $\{q_\phi : \phi \in \Phi\}$ for some parameter space Φ , one can construct the annealing path family of linear paths $q_\phi^{1-t} \pi^t$ from a variational reference to the target π . Similarly, building on the Bézier curve path from earlier, one can consider a parametrized Bézier curve

$$\begin{aligned} \eta_0(t) &= (1-t)((1-t)^2 + 3\phi_{00}(1-t)t + 3\phi_{01}t^2) \\ \eta_1(t) &= t(3\phi_{10}(1-t)^2 + 3\phi_{11}(1-t)t + t^2), \end{aligned}$$

with tunable parameter $\phi = (\phi_{00}, \phi_{01}, \phi_{10}, \phi_{11}) \in \mathbb{R}^4$. If Φ is the subset of $\phi \in \mathbb{R}^4$ such that for all $t \in [0, 1]$, π_t is a normalizable density with the appropriate moment bounds per Definition 1, this is a valid annealing path family.

Since every path in an annealing path family has the desired target distribution π , we are free to optimize the path over the tuning parameter space $\phi \in \Phi$ in addition to optimizing

Algorithm 2 PathOptNRPT

Require: state \mathbf{x} , path family π_t^ϕ , parameter ϕ , # chains N , # PT iterations M , # tuning steps S , learning rate γ
 $\mathcal{T}_N \leftarrow (0, 1/N, 2/N, \dots, 1)$
for $s = 1$ **to** S **do**
 $\{\mathbf{x}_m\}_{m=1}^M, (r_n)_{n=0}^N \leftarrow \text{NRPT}(\mathbf{x}, \pi_t^\phi, \mathcal{T}_N, M)$
 $\lambda^\phi \leftarrow \text{CommunicationBarrier}(\mathcal{T}_N, \{r_n\})$
 $\mathcal{T}_N \leftarrow \text{UpdateSchedule}(\lambda^\phi, N)$
 $\phi \leftarrow \phi - \gamma \nabla_\phi \sum_{n=0}^{N-1} \text{SKL}(\pi_{t_n}^\phi, \pi_{t_{n+1}}^\phi)$
 $\mathbf{x} \leftarrow \mathbf{x}_M$
end for
Return: ϕ, \mathcal{T}_N

the schedule \mathcal{T}_N .² Motivated by the analysis of Section 3.2, a natural objective function for this optimization to consider is the non-asymptotic round trip rate

$$\phi^\star, \mathcal{T}_N^\star = \arg \max_{\phi \in \Phi, \mathcal{T}_N} \tau^\phi(\mathcal{T}_N) \quad (10)$$

$$= \arg \min_{\phi \in \Phi, \mathcal{T}_N} \sum_{n=0}^{N-1} \frac{r^\phi(t_n, t_{n+1})}{1 - r^\phi(t_n, t_{n+1})}, \quad (11)$$

where now the round trip rate and rejection rates depend both on the schedule and path parameter, denoted by superscript ϕ . We solve this optimization using an approximate coordinate-descent procedure, iterating between an update of the schedule \mathcal{T}_N for a fixed path parameter $\phi \in \Phi$, followed by a gradient step in ϕ based on a surrogate objective function and a fixed schedule. This is summarized in Algorithm 2. We outline the details of schedule and path tuning procedure in the following.

Tuning the schedule Fix the value of ϕ , which fixes the path. We adapt a schedule tuning algorithm from past work to update the schedule $\mathcal{T}_N = (t_n)_{n=0}^N$ (Syed et al., 2019, Section 5.1). Based on the same argument as this previous work, we obtain that when $\|\mathcal{T}_N\| \approx 0$, the non-asymptotic round trip rate is maximized when the rejection rates are all equal. The schedule that approximately achieves this satisfies

$$\forall n \in \{1, \dots, N-1\}, \quad \frac{1}{\Lambda^\phi} \int_0^{t_n} \lambda^\phi(s) ds = \frac{n}{N}. \quad (12)$$

We use Monte Carlo estimates of the rejection rates $r^\phi(t_n, t_{n+1})$ in combination with Theorem 2 to approximate $t \mapsto \int_0^t \lambda^\phi(s) ds$, $s \in [0, 1]$, and then use bisection search to solve for each t_n according to Equation (12).

Optimizing the path Fix the schedule \mathcal{T}_N ; we now want to improve the path itself by modifying ϕ . However, this

²We assume that the optimization over ϕ ends after a finite number of iterations to sidestep the potential pitfalls of adaptive MCMC methods (Andrieu & Moulines, 2006).

is not as simple as taking a gradient step for the objective in Equation (10). In particular, it is typical in early iterations when a poor path is initialized that the rejection rates $r^\phi(t_n, t_{n+1}) \approx 1$. As demonstrated empirically in Appendix F, gradient estimates in this regime exhibit a low signal-to-noise ratio that precludes their use for optimization.

Consider instead the global communication barrier $\Lambda^\phi(\mathcal{T}_N)$ for the linear spline approximation to the path; Theorem 2 guarantees that as long as $\|\mathcal{T}_N\|$ is small enough, one can optimize $\Lambda^\phi(\mathcal{T}_N)$ in place of the round trip rate $\tau^\phi(\mathcal{T}_N)$.

First note that by Jensen’s inequality,

$$\frac{1}{N^2} \Lambda^\phi(\mathcal{T}_N)^2 \leq \frac{1}{N} \sum_{n=0}^{N-1} \Lambda^\phi(t_n, t_{n+1})^2.$$

Next, we apply Jensen’s inequality again to the definition of $\Lambda^\phi(t_n, t_{n+1})$ from (5), which shows that

$$\Lambda^\phi(t_n, t_{n+1})^2 \leq \frac{1}{4} \int_0^1 \mathbb{E}[A_{t_n, t_{n+1}}(X_s, X'_s)^2] ds,$$

where X_s are defined in (5) are drawn from the linear path between $\pi_{t_n}^\phi$ and $\pi_{t_{n+1}}^\phi$. Finally, we note that the inner expectation is the path integral of the Fisher information metric along the linear path and evaluates to the symmetric KL divergence (Dabak & Johnson, 2002, Result 4),

$$\int_0^1 \mathbb{E}[(A_{t_n, t_{n+1}}(X_s, X'_s))^2] ds = 2\text{SKL}(\pi_{t_n}^\phi, \pi_{t_{n+1}}^\phi).$$

Therefore we have

$$\frac{2\Lambda^\phi(\mathcal{T}_N)^2}{N} \leq \sum_{n=0}^{N-1} \text{SKL}(\pi_{t_n}^\phi, \pi_{t_{n+1}}^\phi). \quad (13)$$

The slack in this inequality could potentially depend on ϕ even in the large N regime. Therefore, during optimization, we recommend monitoring the value of the original objective function (Equation (10)) to ensure that the optimization of the surrogate SKL objective indeed improves it, and hence the round trip rate performance of PT via Equation (2). In the experiments we display the values of both objective functions.

4. Spline annealing path family

In this section, we develop a family of annealing paths—the *spline annealing path family*—that offers a practical and flexible improvement upon the traditional linear paths considered in past work. We first define a general family of annealing paths based on the exponential family, and then provide the specific details of the spline family with a discussion of its properties. Empirical results in Section 5 demonstrate that the spline annealing path family resolves the problematic Gaussian annealing example in Figure 1.

4.1. Exponential annealing path family

We begin with the practical desiderata for an annealing path family given a fixed reference π_0 and target π_1 distribution.³ First, the traditional linear path $\pi_t \propto \pi_0^{1-t} \pi_1^t$ should be a member of the family, such that one can achieve at least the round trip rate provided by that path. Second, the family should be broadly applicable and not depend on particular details of either π_0 or π_1 . Finally, using the Gaussian example from Figure 1 and Proposition 1 as insight, the family should enable the path to smoothly vary from π_0 to π_1 while inflating / deflating the variance as necessary.

These desiderata motivate the design of the *exponential annealing path family*, in which each annealing path takes the form

$$\pi_t \propto \pi_0^{\eta_0(t)} \pi_1^{\eta_1(t)} = \exp(\eta(t)^T W(x)),$$

for some function $\eta(t) = (\eta_0(t), \eta_1(t))$ and reference/target log densities $W(x) = (W_0(x), W_1(x))$. The Bézier curves from Section 3 are an example. Intuitively, $\eta_0(t)$ and $\eta_1(t)$ represent the level of annealing for the reference and target respectively along the path. Proposition 2 shows that a broad collection of functions η indeed construct a valid annealing path family including the linear path. Without loss of generality, we assume any piecewise twice continuously differentiable function $\eta : [0, 1] \rightarrow \mathbb{R}^2$ is reparameterized such that for $t \in [0, 1]$ where $\eta'(t)$ exists, $\|\eta'(t)\|_2 = L$ where L is the length of the path.

Proposition 2. *Let $\Omega \subseteq \mathbb{R}^2$ be the set*

$$\Omega = \left\{ \xi \in \mathbb{R}^2 : \int \exp(\xi^T W(x)) (1 + \|W(x)\|_2^3) dx < \infty \right\}.$$

Suppose $(0, 1) \in \Omega$ and \mathcal{A}_M is the set of piecewise twice continuously differentiable functions $\eta : [0, 1] \rightarrow \Omega$ such that $\eta(1) = (0, 1)$ and $\sup_t \|\eta''(t)\|_2 \leq M$. Then

$$\{\pi_t(x) \propto \exp(\eta(t)^T W(x)) : \eta \in \mathcal{A}_M\}$$

is an annealing path family for target distribution π_1 . Moreover, if $(1, 0) \in \Omega$, then \mathcal{A}_M contains the linear path $\pi_t \propto \pi_0^{1-t} \pi_1^t$.

4.2. Spline annealing path family

Proposition 2 reduces the problem of designing a general family of paths of probability distributions to the much simpler task of designing paths in \mathbb{R}^2 . We argue that a good choice can be constructed using linear spline paths connecting K knots $\phi = (\phi_0, \dots, \phi_K) \in (\mathbb{R}^2)^{K+1}$, i.e., for all $k \in \{1, \dots, K\}$ and $t \in [\frac{k-1}{K}, \frac{k}{K}]$,

$$\eta^\phi(t) \mapsto (k - Kt)\phi_{k-1} + (Kt - k + 1)\phi_k.$$

³A natural extension of this discussion would include parametrized variational reference distribution families. For simplicity we restrict to a fixed reference.

Let Ω be defined in Proposition 2. The K -knot *spline annealing path family* is defined as the set of K -knot linear spline paths such that

$$\phi_0 = (1, 0), \quad \phi_K = (0, 1), \quad \text{and} \quad \forall k, \phi_k \in \Omega.$$

Validity: Since Ω is a convex set per the proof of Proposition 2, we are guaranteed that $\eta^\phi([0, 1]) \subseteq \Omega$, and so this collection of annealing paths is a subset of the exponential annealing family and hence forms a valid annealing path family targeting π_1 .

Convexity: Furthermore, convexity of Ω implies that tuning the knots $\phi \in \Omega^{K+1}$ involves optimization within a convex constraint set. In practice, we enforce also that the knots are monotone in each component—i.e., the first component monotonically decreases $1 \rightarrow 0$ and the second increases $0 \rightarrow 1$ —such that the path of distributions always moves from the reference to the target. Because monotonicity constraint sets are linear and hence convex, the overall monotonicity-constrained optimization problem has a convex domain.

Flexibility: Assuming the family is nonempty, it trivially contains the linear path. Further, given a large enough number of knots K , the spline annealing family well-approximates subsets of the exponential annealing family for fixed $M > 0$. In particular,

$$\sup_{\eta \in \mathcal{A}_M} \inf_{\phi \in \Omega^{K+1}} \|\eta^\phi - \eta\|_\infty \leq \frac{M}{4K^2}. \quad (14)$$

Figure 2 provides an illustration of the behaviour of optimized spline paths for a Gaussian reference and target. The path takes a convex curved shape; starting at the bottom right point of the figure (reference), this path corresponds to increasing the variance of the reference, shifting the mean from reference to target, and finally decreasing the variance to match the target. With more knots, this process happens more smoothly.

Appendix D provides an explicit derivation of the stochastic gradient estimates we use to optimize the knots of the spline annealing path family. It is also worth making two practical notes. First, we cannot use the usual 2-norm projection to enforce the constraint, because this causes an undesirable collapse of knots. Therefore, we maintain monotonicity as follows: after each stochastic gradient step, we identify a monotone subsequence of knots containing the endpoints, remove the nonmonotone jumps, and linearly interpolate between the knot subsequence with an even spacing. Second, we take gradient steps in a log-transformed space such that knot components are always strictly positive.

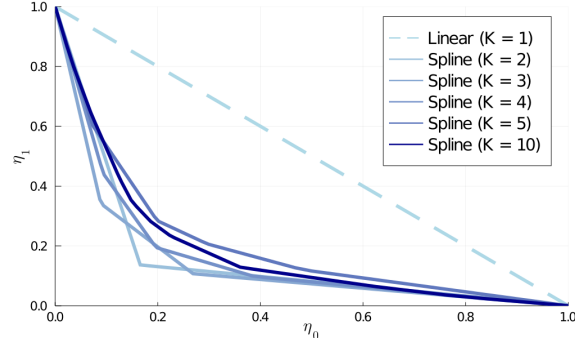


Figure 2. The spline path for $K = 1, 2, 3, 4, 5, 10$ knots for the family generated by $\pi_0 = N(-1, 0.5)$ and $\pi_1 = N(1, 0.5)$.

5. Experiments

In this section, we study the empirical performance of non-reversible PT based on the spline annealing path family ($K \in \{2, 3, 4, 5, 10\}$) from Section 4, with knots and schedule optimized using the tuning method from Section 3. We compare this method to two PT methods based on standard linear paths: non-reversible PT with adaptive schedule (“NRPT+Linear”) (Syed et al., 2019), and reversible PT (“Reversible+Linear”) (Atchadé et al., 2011).

We use the terminology “scan” to denote one iteration of the for loop in Algorithm 2. The computational cost of a scan is comparable for all the methods, since the bottleneck is the local exploration step shared by all methods. These experiments demonstrate two primary conclusions: (1) tuned nonlinear paths provide a substantially higher round trip rate compared to linear paths for the examples considered; and (2) the symmetric KL sum objective (Equation 13) is a good proxy for the round trip rate as a tuning objective.

We run the following benchmark problems; see the supplement for details. **Gaussian:** a synthetic setup in which the reference distribution is $\pi_0 = N(-1, 0.01^2)$ and the target is $\pi_1 = N(1, 0.01^2)$. For this example we used $N = 50$ parallel chains and fixed the computational budget to 45000 samples. For Algorithm 2, the computational budget was divided equally over 150 scans, meaning 300 samples were used for every gradient update. “Reversible+Linear” performed 45000 local exploration steps with a communication step after every iteration while for “NRPT+Linear” the computational budget was used to adapt the schedule. The gradient updates were performed using Adagrad with learning rate equal to 0.2. **Beta-binomial model:** a conjugate Bayesian model with prior $\pi_0(p) = \text{Beta}(180, 840)$ and likelihood $L(x|p) = \text{Binomial}(x|n, p)$. We simulated data $x_1, \dots, x_{2000} \sim \text{Binomial}(100, 0.7)$ resulting in a posterior $\pi_1(p) = \text{Beta}(140180, 60840)$. The prior and posterior are heavily concentrated at 0.2 and 0.7 respectively.

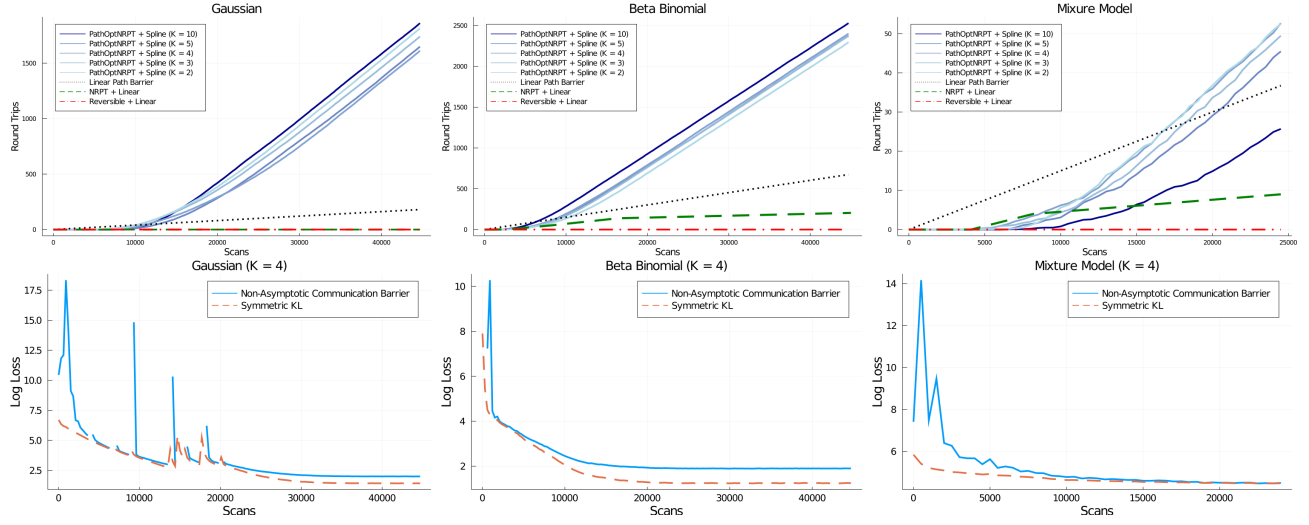


Figure 3. Top: Cumulative round trips averaged over 10 runs for the spline path with $K = 2, 3, 4, 5, 10$ (solid blue), NRPT using a linear path (dashed green), and reversible PT with linear path (dash/dot red). The slope of the lines represent the round trip rate. We observe large gains going from linear to non-linear paths ($K > 1$). For all values of $K > 1$, the optimized spline path substantially improves on the theoretical upper bound on round trip rate possible using linear path (dotted black). **Bottom:** Non-asymptotic communication barrier from Equation 11 (solid blue) and Symmetric KL (dash orange) as a function of iteration for one run of PathOptNRPT + Spline ($K = 4$ knots).

We used the same settings as for the Gaussian example.

Mixture model: A Bayesian Gaussian mixture model with mixture proportions w_0, w_1 , mixture component densities $N(\mu_i, 10^2)$ for mean parameters μ_0, μ_1 , and a binary cluster label for each data point. We place a $\text{Dir}(1, 1)$ prior on the proportions, and a $N(150, 1)$ prior on each of the two mean parameters. We simulated $n = 1000$ data points from the mixture $0.3N(100, 10^2) + 0.7N(200, 10^2)$. Exploring the full posterior distribution is challenging in this context due to a combination of misspecification of the prior and label switching. In this example we used $N = 35$ chains and fixed the computational budget to 25000, divided into 50 scans using 500 samples each. We optimize the path using Adagrad with a learning rate of 0.3. For all the experiments we performed one local exploration step before each communication step.

The results of these experiments are shown in Figure 3. Examining the top row—which shows the number of round trips as a function of the number of scans—one can see that PT using the spline annealing family outperforms PT using the linear annealing path across all numbers of knots tested. Moreover, the slope of these curves demonstrates that PT with the spline annealing family exceeds the theoretical upper bound of round trip rate for the linear annealing path (from Equation (8)). The largest gain is obtained from going from $K = 1$ (linear) to $K = 2$. For the Gaussian and beta-binomial examples, increasing the number of knots to more than $K > 2$ leads to marginal improvements. In the

case of the Gaussian example, note that since the global communication barrier Λ for the linear path is much larger than N , algorithms based on linear paths incurred rejection rates of nearly one for most chains, resulting in no round trips. For the mixture example, we note that once one adds a large number ($K = 10$) of knots, the path optimization proceeds more slowly.

The bottom row of Figure 3 shows the value of the surrogate SKL objective and non-asymptotic communication barrier from Equation 11. In particular, these figures demonstrate that the SKL provides a surrogate objective that is a reasonable proxy for the non-asymptotic communication barrier, but does not exhibit as large estimation variance in early iterations when there are pairs of chains with rejection rates close to one.

6. Discussion

In this work, we identified the use of linear paths of distributions as a major bottleneck in the performance of parallel tempering algorithms. To address this limitation, we have provided a theory of parallel tempering on nonlinear paths, a methodology to tune parametrized paths, and finally a practical, flexible family of paths based on linear splines. Future work in this line of research includes extensions to estimate normalization constants, as well as the development of techniques and theory surrounding the use of variational reference distributions.

References

- Andrieu, C. and Moulines, E. On the ergodicity properties of some adaptive MCMC algorithms. *Annals of Applied Probability*, 16(3):1462–1505, 2006.
- Atchadé, Y. F., Roberts, G. O., and Rosenthal, J. S. Towards optimal scaling of Metropolis-coupled Markov chain Monte Carlo. *Statistics and Computing*, 21(4): 555–568, 2011.
- Ballnus, B., Hug, S., Hatz, K., Görlitz, L., Hasenauer, J., and Theis, F. J. Comprehensive benchmarking of Markov chain Monte Carlo methods for dynamical systems. *BMC Systems Biology*, 11(1):63, 2017.
- Brekelmans, R., Masrani, V., Bui, T., Wood, F., Galstyan, A., Steeg, G. V., and Nielsen, F. Annealed importance sampling with q-paths. *arXiv:2012.07823*, 2020.
- Costa, S. I., Santos, S. A., and Strapasson, J. E. Fisher information distance: A geometrical reading. *Discrete Applied Mathematics*, 197:59–69, 2015.
- Dabak, A. G. and Johnson, D. H. Relations between Kullback-Leibler distance and Fisher information. *Journal of The Iranian Statistical Society*, 5:25–37, 2002.
- Desjardins, G., Luo, H., Courville, A., and Bengio, Y. Deep tempering. *arXiv:1410.0123*, 2014.
- Gelman, A. and Meng, X.-L. Simulating normalizing constants: From importance sampling to bridge sampling to path sampling. *Statistical science*, pp. 163–185, 1998.
- Geyer, C. J. Markov chain Monte Carlo maximum likelihood. *Interface Proceedings*, 1991.
- Grosse, R. B., Maddison, C. J., and Salakhutdinov, R. R. Annealing between distributions by averaging moments. In *Advances in Neural Information Processing Systems*, 2013.
- Kamberaj, H. *Molecular Dynamics Simulations in Statistical Physics: Theory and Applications*. Springer, 2020.
- Lingenheil, M., Denschlag, R., Mathias, G., and Tavan, P. Efficiency of exchange schemes in replica exchange. *Chemical Physics Letters*, 478(1-3):80–84, 2009.
- Müller, N. F. and Bouckaert, R. R. Adaptive parallel tempering for BEAST 2. *bioRxiv*, 2020. doi: 10.1101/603514.
- Okabe, T., Kawata, M., Okamoto, Y., and Mikami, M. Replica-exchange Monte Carlo method for the isobaric–isothermal ensemble. *Chemical Physics Letters*, 335(5-6): 435–439, 2001.
- Predescu, C., Predescu, M., and Ciobanu, C. V. The incomplete beta function law for parallel tempering sampling of classical canonical systems. *The Journal of Chemical Physics*, 120(9):4119–4128, 2004.
- Rainforth, T., Kosiorek, A. R., Le, T. A., Maddison, C. J., Igl, M., Wood, F., and Teh, Y. W. Tighter variational bounds are not necessarily better. In *International Conference on Machine Learning*, 2018.
- Rischar, M., Jacob, P. E., and Pillai, N. Unbiased estimation of log normalizing constants with applications to Bayesian cross-validation. *arXiv:1810.01382*, 2018.
- Sakai, Y. and Hukushima, K. Irreversible simulated tempering. *Journal of the Physical Society of Japan*, 85(10): 104002, 2016.
- Syed, S., Bouchard-Côté, A., Deligiannidis, G., and Doucet, A. Non-reversible parallel tempering: an embarrassingly parallel MCMC scheme. 2019. *arXiv:1905.02939*.
- Tawn, N. G., Roberts, G. O., and Rosenthal, J. S. Weight-preserving simulated tempering. *Statistics and Computing*, 30(1):27–41, 2020.
- Woodard, D. B., Schmidler, S. C., Huber, M., et al. Conditions for rapid mixing of parallel and simulated tempering on multimodal distributions. *The Annals of Applied Probability*, 19(2):617–640, 2009.
- Zhou, Y., Johansen, A. M., and Aston, J. A. Toward automatic model comparison: An adaptive sequential Monte Carlo approach. *Journal of Computational and Graphical Statistics*, 25(3):701–726, 2016.

A. Proof of Proposition 1

Define $\pi_0 = N(\mu_0, \sigma^2)$ and $\pi_1 = N(\mu_1, \sigma^2)$ with $W_i(x) \propto -\frac{1}{2\sigma^2}(x - \mu_i)^2$ (throughout we use the proportionality symbol \propto with log-densities to indicate an unspecified additive constant). Suppose π_t is the linear path $\pi_t(x) \propto \exp(W_t)$ where $W_t = (1-t)W_0 + tW_1$. Note that as a function of x ,

$$\begin{aligned} W_t(x) &\propto -\frac{1-t}{2\sigma^2}(x - \mu_0)^2 - \frac{t}{2\sigma^2}(x - \mu_1)^2 \\ &\propto -\frac{1}{2\sigma^2}(x - \mu_t)^2, \quad \mu_t = (1-t)\mu_0 + t\mu_1, \end{aligned}$$

and thus $\pi_t = N(\mu_t, \sigma^2)$. Taking a derivative of W_t , we find that

$$\frac{dW_t}{dt} = \frac{(\mu_1 - \mu_0)(x - \frac{\mu_0 + \mu_1}{2})}{\sigma^2}.$$

We will now compute $\lambda(t)$. If $X_t, X'_t \sim \pi_t$, then

$$\begin{aligned} \lambda(t) &= \frac{1}{2} \mathbb{E} \left[\left| \frac{dW}{dt}(X_t) - \frac{dW}{dt}(X'_t) \right| \right] \\ &= \frac{|\mu_1 - \mu_0|}{2\sigma} \mathbb{E} \left[\left| \frac{X_t - \frac{\mu_0 + \mu_1}{2}}{\sigma} - \frac{X'_t - \frac{\mu_0 + \mu_1}{2}}{\sigma} \right| \right] \\ &= \frac{|\mu_1 - \mu_0|}{2\sigma} \mathbb{E} \left[\left| \frac{X_t - \mu_t}{\sigma} - \frac{X'_t - \mu_t}{\sigma} \right| \right] \\ &= \frac{|\mu_1 - \mu_0|}{2\sigma} \mathbb{E} [|Z - Z'|], \end{aligned}$$

where $Z, Z' \sim N(0, 1)$. Thus $Z - Z' \sim N(0, 2)$, and $|Z - Z'|$ has a folded normal distribution with expectation $2/\sqrt{\pi}$. This implies $\lambda(t) = z/\sqrt{\pi}$ where $z = |\mu_1 - \mu_0|/\sigma$ and $\Lambda = \int_0^1 \lambda(t) dt = z/\sqrt{\pi}$. By Theorem 2, the asymptotic round trip rate $\tau_\infty^{\text{linear}}$ for the linear path satisfies,

$$\tau_\infty^{\text{linear}} = \frac{1}{2 + 2\Lambda} = \frac{1}{2 + 2z/\sqrt{\pi}} = \Theta\left(\frac{1}{z}\right).$$

We will now establish an upper bound for the communication barrier Λ for a general path π_t . If $X_t, X'_t \sim \pi_t$, then Theorem 2 and Jensen's inequality imply the following:

$$\begin{aligned} \Lambda &= \int_0^1 \frac{1}{2} \mathbb{E} \left[\sqrt{\left(\frac{dW}{dt}(X_t) - \frac{dW}{dt}(X'_t) \right)^2} \right] dt \\ &\leq \int_0^1 \frac{1}{2} \sqrt{\mathbb{E} \left[\left(\frac{dW}{dt}(X_t) - \frac{dW}{dt}(X'_t) \right)^2 \right]} dt \\ &= \frac{1}{\sqrt{2}} \int_0^1 \sqrt{\text{Var}_{\pi_t} \left[\frac{dW_t}{dt} \right]} dt \\ &= \frac{1}{\sqrt{2}} \Lambda_F, \end{aligned}$$

where Λ_F is the length of the the path π_t with the Fisher information metric. The geodesic path of Gaussians between π_0 and π_1 that minimizes Λ_F satisfies (Costa et al., 2015, Eq. 11, Sec. 2)

$$\Lambda_F = \sqrt{2} \log \left(1 + \frac{z^2}{4} + \frac{z}{4} \sqrt{8 + z^2} \right). \quad (15)$$

Again, by Theorem 2, the asymptotic round trip rate $\tau_\infty^{\text{geodesic}}$ for the geodesic path satisfies

$$\tau_\infty^{\text{geodesic}} = \frac{1}{2 + 2\Lambda} \geq \frac{1}{2 + 2\Lambda_F} = \Theta\left(\frac{1}{\log z}\right).$$

B. Proof of Lemma 1

Definition 4. Given a path π_t and measurable function f , we denote $\|f\|_\pi = \sup_t \mathbb{E}_{\pi_t}[f]$.

Following the computation in Predescu et al. (2004, Proposition 1), we have

$$r(t, t') = 1 - \frac{\mathbb{E}[\exp(-\frac{1}{2}|A_{t,t'}(\tilde{X}_{1/2}, \tilde{X}'_{1/2})|)]}{\mathbb{E}[\exp(-\frac{1}{2}A_{t,t'}(\tilde{X}_{1/2}, \tilde{X}'_{1/2}))]}, \quad (16)$$

where $\tilde{X}_s, \tilde{X}'_s \sim \tilde{\pi}_s = \frac{1}{Z(s)} \exp((1-s)W_t + sW_{t'})$ and

$$A_{t,t'}(x, x') = (W_{t'}(x) - W_t(x)) - (W_{t'}(x') - W_t(x')).$$

In particular, the path of distributions $\tilde{\pi}_s$ for $s \in [0, 1]$ is the linear path between π_t and $\pi_{t'}$.

Lemma 2. For all $k \geq 1$, there is a (possibly infinite) constant \tilde{C}_k independent of t, t', \mathcal{T}_N such that

$$\sup_s \mathbb{E}[|A_{t,t'}(\tilde{X}_s, \tilde{X}'_s)|^k] \leq \tilde{C}_k |t' - t|^k.$$

where $\tilde{X}_s, \tilde{X}'_s \sim \tilde{\pi}_s$.

Proof. The mean-value theorem and condition 3 of Definition 1 imply that $W_t(x)$ is Lipschitz in t ,

$$|W_t(x) - W_{t'}(x)| \leq V_1(x) |t' - t|.$$

The triangle inequality therefore implies

$$|A_{t,t'}(x, x')| \leq (V_1(x) + V_1(x')) |t' - t|.$$

By taking expectations and using the fact $|a + b|^k \leq 2^{k-1}(|a|^k + |b|^k)$, we have that

$$\begin{aligned} \mathbb{E}[|A_{t,t'}(\tilde{X}_s, \tilde{X}'_s)|^k] &\leq 2^k \mathbb{E}_{\tilde{\pi}_s}[V_1^k] |t' - t|^k \\ &\leq 2^k \|V_1^k\|_{\tilde{\pi}_s} |t' - t|^k. \end{aligned}$$

□

We now begin the proof of Lemma 1. Define $\tilde{\lambda}(s) = \frac{1}{2}\mathbb{E}[|A_{t,t'}(\tilde{X}_s, \tilde{X}'_s)|]$ for $\tilde{X}_s, \tilde{X}'_s \sim \tilde{\pi}_s$. Then a third order Taylor expansion of Equation (16) (Predescu et al., 2004), which contains terms of the form $\mathbb{E}[|A_{t,t'}(\tilde{X}_s, \tilde{X}'_s)|^k]$ that can be controlled via Lemma 2, yields

$$r(t, t') = \tilde{\lambda}(1/2) + R(t, t'), \quad |R(t, t')| \leq C'|t - t'|^3,$$

for some finite constant C' independent of t, t' . By Syed et al. (2019, Prop. 2, Appendix C) we have that in addition, $\tilde{\lambda}(s)$ is in $C^2([0, 1])$, and thus there is a constant C'' independent of t, t' such that

$$\sup_s \left| \frac{d^2 \tilde{\lambda}}{ds^2} \right| \leq C''|t - t'|^3.$$

The error bound for the midpoint rule implies,

$$\begin{aligned} \left| \tilde{\lambda}(1/2) - \int_0^1 \tilde{\lambda}(s) ds \right| &\leq \frac{1}{24} \sup_s \left| \frac{d^2 \tilde{\lambda}}{ds^2} \right| \\ &\leq \frac{C''}{24} |t - t'|^3. \end{aligned}$$

The result follows: there is a finite constant C independent of t, t' such that

$$|r(t, t') - \Lambda(t, t')| = \left| r(t, t') - \int_0^1 \tilde{\lambda}(s) ds \right| \leq C|t' - t|^3.$$

C. Proof of Theorem 2

We first note that without loss of generality we can place an artificial schedule point t_n at each of the finitely many discontinuities in W_t or its first/second derivative. Thus we assume the W_t is C^2 on each interval $[t_{n-1}, t_n]$. Later in the proof it will become clear that the contributions of these artificial schedule points becomes negligible as $\|\mathcal{T}_N\| \rightarrow 0$.

Given a schedule \mathcal{T}_N , define the path $\tilde{\pi}_t = \frac{1}{\tilde{Z}_t} \exp(\tilde{W}_t)$ with log-likelihood \tilde{W}_t satisfying for each segment $t_{n-1} \leq t \leq t_n$,

$$\tilde{W}_t = W_{t_{n-1}} + \frac{\Delta W_n}{\Delta t_n} (t - t_{n-1}),$$

where $\Delta W_n = W_{t_n} - W_{t_{n-1}}$ and $\Delta t_n = t_n - t_{n-1}$. In particular, \tilde{W}_t agrees with W_t for $t \in \mathcal{T}_N$, linearly interpolates between $W_{t_{n-1}}$ and W_{t_n} for $t \in [t_{n-1}, t_n]$, and for all x ,

$$|\tilde{W}_t(x) - W_t(x)| \leq \frac{1}{2} \sup_{t \in [t_{n-1}, t_n]} \left| \frac{d^2 W_t}{dt^2}(x) \right| \Delta t_n^2. \quad (17)$$

The following lemma shows that the normalization constant of, and expectations under, $\tilde{\pi}_t$ are comparable to the same for π_t with an error bound that depends on $\|\mathcal{T}_N\|$ and converges to 0 as $\|\mathcal{T}_N\| \rightarrow 0$.

Lemma 3. For measurable functions f and $s > 0$, let

$$E_t(f, s) = \mathbb{E}_{\pi_t} \left[|f| e^{s^2 V_2} \right],$$

and define $E_t(s) = E_t(1, s)$ for brevity.

(a) For any schedule \mathcal{T}_N ,

$$\left| \frac{\tilde{Z}_t}{Z_t} - 1 \right| \leq E_t(\|\mathcal{T}_N\|) - 1,$$

and if $\|\mathcal{T}_N\|$ is small enough that $E_t(\|\mathcal{T}_N\|) < 2$,

$$\left| \frac{Z_t}{\tilde{Z}_t} - 1 \right| \leq \frac{E_t(\|\mathcal{T}_N\|) - 1}{2 - E_t(\|\mathcal{T}_N\|)}.$$

(b) For any schedule \mathcal{T}_N and measureable function f , if $\|\mathcal{T}_N\|$ is small enough that $E_t(\|\mathcal{T}_N\|) < 2$,

$$\begin{aligned} |\mathbb{E}_{\tilde{\pi}_t}[f] - \mathbb{E}_{\pi_t}[f]| &\leq \frac{E_t(\|\mathcal{T}_N\|) - 1}{2 - E_t(\|\mathcal{T}_N\|)} E_t(f, \|\mathcal{T}_N\|) \\ &\quad + E_t(f, \|\mathcal{T}_N\|) - E_t(f, 0). \end{aligned}$$

Proof. (a) We rewrite the expression

$$\begin{aligned} \frac{\tilde{Z}_t}{Z_t} &= \frac{1}{Z_t} \int_{\mathcal{X}} e^{\tilde{W}_t(x)} dx \\ &= \int_{\mathcal{X}} e^{\tilde{W}_t(x) - W_t(x)} \pi_t(x) dx \\ &= 1 + \int_{\mathcal{X}} \left(e^{\tilde{W}_t(x) - W_t(x)} - 1 \right) \pi_t(x) dx. \end{aligned}$$

Thus using the inequality $|e^x - 1| \leq e^{|x|} - 1$,

$$\begin{aligned} \left| \frac{\tilde{Z}_t}{Z_t} - 1 \right| &\leq \left| \int_{\mathcal{X}} \left(e^{\tilde{W}_t(x) - W_t(x)} - 1 \right) \pi_t(x) dx \right| \\ &\leq \int_{\mathcal{X}} \left(e^{|\tilde{W}_t(x) - W_t(x)|} - 1 \right) \pi_t(x) dx \\ &\leq \int_{\mathcal{X}} \left(e^{V_2(x) \|\mathcal{T}_N\|^2} - 1 \right) \pi_t(x) dx \\ &= \mathbb{E}_{\pi_t} \left[e^{\|\mathcal{T}_N\|^2 V_2} - 1 \right] \\ &= E_t(\|\mathcal{T}_N\|) - 1. \end{aligned}$$

The bound on $|Z_t/\tilde{Z}_t - 1|$ arises from straightforward algebraic manipulation of the above bound.

(b) We begin by rewriting $\mathbb{E}_{\tilde{\pi}_t}[f]$:

$$\begin{aligned} \mathbb{E}_{\tilde{\pi}_t}[f] - \mathbb{E}_{\pi_t}[f] &= \frac{1}{\tilde{Z}_t} \int_{\mathcal{X}} f(x) e^{\tilde{W}_t(x)} dx - \mathbb{E}_{\pi_t}[f] \\ &= \int_{\mathcal{X}} f(x) \left(\frac{Z_t}{\tilde{Z}_t} e^{\tilde{W}_t(x) - W_t(x)} - 1 \right) \pi_t(x) dx \\ &= \left(\frac{Z_t}{\tilde{Z}_t} - 1 \right) \int_{\mathcal{X}} f(x) e^{\tilde{W}_t(x) - W_t(x)} \pi_t(x) dx \\ &\quad + \int_{\mathcal{X}} f(x) \left(e^{\tilde{W}_t(x) - W_t(x)} - 1 \right) \pi_t(x) dx. \end{aligned}$$

Therefore again using $|e^x - 1| \leq e^{|x|} - 1$ and the previous bound,

$$\begin{aligned} |\mathbb{E}_{\tilde{\pi}_t}[f] - \mathbb{E}_{\pi_t}[f]| &\leq \frac{E_t(\|\mathcal{T}_N\|) - 1}{2 - E_t(\|\mathcal{T}_N\|)} E_t(f, \|\mathcal{T}_N\|) \\ &\quad + E_t(f, \|\mathcal{T}_N\|) - E_t(f, 0). \end{aligned}$$

□

By changing variables via $t = t_{n-1} + s\Delta t_n$ in (5), we can rewrite $\Lambda(t_{n-1}, t_n)$ as

$$\Lambda(t_{n-1}, t_n) = \int_{t_{n-1}}^{t_n} \frac{1}{2} \mathbb{E} \left[\left\| \frac{\Delta W_n}{\Delta t_n}(\tilde{X}_t) - \frac{\Delta W_n}{\Delta t_n}(\tilde{X}'_t) \right\| \right] dt,$$

where $\tilde{X}_t, \tilde{X}'_t \sim \tilde{\pi}_t$. Note that by construction for $t \in (t_{n-1}, t_n)$ we have $\frac{d\tilde{W}_t}{dt}$ exists and equals $\frac{\Delta W_n}{\Delta t_n}$. So by summing over n we get,

$$\begin{aligned} \Lambda(\mathcal{T}_N) &= \sum_{n=1}^N \Lambda(t_{n-1}, t_n) \\ &= \int_0^1 \frac{1}{2} \mathbb{E} \left[\left\| \frac{d\tilde{W}_t}{dt}(\tilde{X}_t) - \frac{d\tilde{W}_t}{dt}(\tilde{X}'_t) \right\| \right] dt \\ &= \int_0^1 \tilde{\lambda}(t) dt \end{aligned}$$

If we can show that $\sup_t |\tilde{\lambda}(t) - \lambda(t)|$ converges uniformly⁴ to 0 as $\|\mathcal{T}_N\| \rightarrow 0$ then by dominated convergence theorem $\Lambda(\mathcal{T}_N)$ converges to Λ uniformly as $\|\mathcal{T}_N\| \rightarrow 0$. The round trip rate then uniformly converges to $(2+2\Lambda)^{-1}$ by Theorem 3 of (Syed et al., 2019).

Adding and subtracting $\mathbb{E} \left[\left\| \frac{d\tilde{W}_t}{dt}(X_t) - \frac{d\tilde{W}_t}{dt}(X'_t) \right\| \right]$ within the absolute difference $2|\tilde{\lambda}(t) - \lambda(t)|$ and using the triangle inequality, it can be shown that we require bounds on

$$J_{1,t} = \int \pi_t(x) \pi_t(y) \left| \left| \frac{d\tilde{W}_t}{dt}(x) - \frac{d\tilde{W}_t}{dt}(y) \right| - \left| \frac{dW_t}{dt}(x) - \frac{dW_t}{dt}(y) \right| \right|$$

⁴We say $a(\mathcal{T}_N)$ converges uniformly to a if for all $\epsilon > 0$, $\exists \delta > 0$ such that $\|\mathcal{T}_N\| < \delta$ implies $|a(\mathcal{T}_N) - a| < \epsilon$.

and

$$J_{2,t} = \int |\pi_t(x) \pi_t(y) - \tilde{\pi}_t(x) \tilde{\pi}_t(y)| \left| \frac{d\tilde{W}_t}{dt}(x) - \frac{d\tilde{W}_t}{dt}(y) \right|.$$

For the first term, the mean value theorem implies that there exist $s, s' \in [t_{n-1}, t_n]$ (potentially functions of x and y , respectively) such that

$$J_{1,t} = \int \pi_t(x) \pi_t(y) \left| \left| \frac{dW_s}{dt}(x) - \frac{dW_{s'}}{dt}(y) \right| - \left| \frac{dW_t}{dt}(x) - \frac{dW_t}{dt}(y) \right| \right|$$

Split the integral into the set A of $x, y \in \mathcal{X}$ where the first term in the absolute value is larger; the same analysis with the same result applies in the other case in A^c . Here, Taylor's theorem and the triangle inequality yield

$$\begin{aligned} \left| \frac{dW_s}{dt}(x) - \frac{dW_{s'}}{dt}(y) \right| &\leq \left| \frac{dW_t}{dt}(x) - \frac{dW_t}{dt}(y) \right| \\ &\quad + (V_2(x) + V_2(y)) \|\mathcal{T}_N\|. \end{aligned}$$

Using this and the same procedure for A^c , we have that

$$\begin{aligned} J_{1,t} &\leq \int \pi_t(x) \pi_t(y) (V_2(x) + V_2(y)) \|\mathcal{T}_N\| \\ &= 2\mathbb{E}_{\pi_t}[V_2] \|\mathcal{T}_N\|. \end{aligned}$$

This converges to 0 as $\|\mathcal{T}_N\| \rightarrow 0$.

For the second term $J_{2,t}$, we can again use the mean value theorem to find $s, s' \in [t_{n-1}, t_n]$ where

$$J_{2,t} = \int |\pi_t(x) \pi_t(y) - \tilde{\pi}_t(x) \tilde{\pi}_t(y)| \left| \frac{dW_s}{dt}(x) - \frac{dW_{s'}}{dt}(y) \right|,$$

and therefore via the triangle inequality, symmetry, and the $V_1(x)$ bound on the first path derivative,

$$J_{2,t} \leq 2 \int V_1(x) |\pi_t(x) \pi_t(y) - \tilde{\pi}_t(x) \tilde{\pi}_t(y)|.$$

We then add and subtract $\pi(x)\tilde{\pi}(y)$ within the absolute value and use the triangle inequality again to find that

$$\begin{aligned} J_{2,t} &\leq 2 \int (V_1(x) + \mathbb{E}_{\pi_t}[V_1]) |\pi_t(x) - \tilde{\pi}_t(x)| \\ &= 2 \int \pi_t(x) (V_1(x) + \mathbb{E}_{\pi_t}[V_1]) \left| 1 - \frac{\tilde{\pi}_t(x)}{\pi_t(x)} \right|. \end{aligned}$$

Note that by the triangle inequality and the bound $|e^x - 1| \leq e^{|x|} - 1$,

$$\left| 1 - \frac{\tilde{\pi}_t(x)}{\pi_t(x)} \right| \leq \left| \frac{Z_t}{\tilde{Z}_t} - 1 \right| e^{\|\mathcal{T}_N\|^2 V_2(x)} + e^{\|\mathcal{T}_N\|^2 V_2(x)} - 1.$$

Assume that $\|\mathcal{T}_N\|$ is small enough such that $E_t(\|\mathcal{T}_N\|) < 2$, and let $f = V_1 + \mathbb{E}_{\pi_t}[V_1]$. Then by Lemma 3,

$$\begin{aligned} J_{2,t} &\leq 2 \frac{E_t(\|\mathcal{T}_N\|) - 1}{2 - E_t(\|\mathcal{T}_N\|)} E_t(f, \|\mathcal{T}_N\|) \\ &\quad + E_t(f, \mathcal{T}_N) - E_t(f, 0). \end{aligned}$$

By assumption we know that $E_t(f, s)$ is finite for some s small enough. Therefore as $\|\mathcal{T}_N\| \rightarrow 0$, by monotone convergence $E_t(f, \|\mathcal{T}_N\|) \rightarrow E_t(f, 0)$, and in particular $E_t(\mathcal{T}_N) \rightarrow 1$. Therefore $J_{1,t} + J_{2,t} \rightarrow 0$ as $\|\mathcal{T}_N\| \rightarrow 0$ and the proof is complete.

D. Objective and Gradient

Here we derive the gradient used to optimize the surrogate SKL objective in Equation 13. First we derive the gradient for the expectation of a general function in Section D.1. Next, in Section D.2, we show the result for the specific case of expectations of linear functions with respect to distributions in the exponential family. Lastly, we show how the result is related to our SKL objective in Sections D.3 and D.4.

D.1. Derivative of parameter-dependent expectation

Here we consider the problem of computing

$$g_\phi(x) = \nabla_\phi \int_{\mathcal{X}} \pi_\phi(x) J_\phi(x) dx$$

where $\pi_\phi(x) = Z(\phi)^{-1} \exp(W_\phi(x))$, $Z(\phi) = \int_{\mathcal{X}} \exp(W_\phi(x)) dx$ and $J_\phi(x)$ is a function depending on ϕ . Assuming we can interchange the gradient and the expectation and using the product rule we can rewrite:

$$g_\phi(x) = \int_{\mathcal{X}} (J_\phi(x) \nabla_\phi \pi_\phi(x) + \pi_\phi(x) \nabla_\phi J_\phi(x)) dx.$$

Using $\nabla_\phi \pi_\phi(x) = \pi_\phi(x) \nabla_\phi \log \pi_\phi(x)$,

$$g_\phi(x) = \int_{\mathcal{X}} \pi_\phi(x) (J_\phi(x) \nabla_\phi \log \pi_\phi(x) + \nabla_\phi J_\phi(x)) dx.$$

From the definition of $\pi_\phi(x)$, we can evaluate the score function as

$$\begin{aligned} \nabla_\phi \log \pi_\phi(x) &= -\nabla_\phi \log Z(\phi) + \nabla_\phi W_\phi(x) \\ &= -\mathbb{E}[\nabla_\phi W_\phi(x)] + \nabla_\phi W_\phi(x). \end{aligned}$$

Substitute this in $g_\phi(x)$ we obtain,

$$\begin{aligned} g_\phi(x) &= \int_{\mathcal{X}} \pi_\phi(x) J_\phi(x) (-\mathbb{E}[\nabla_\phi W_\phi(x)] + \nabla_\phi W_\phi(x)) dx \\ &\quad + \int_{\mathcal{X}} \pi_\phi(x) \nabla_\phi J_\phi(x) dx \\ &= -\mathbb{E}[J_\phi(x) \mathbb{E}[\nabla_\phi W_\phi(x)]] + \mathbb{E}[J_\phi(x) \nabla_\phi W_\phi(x)] \\ &\quad + \mathbb{E}[\nabla_\phi J_\phi(x)] \\ &= \text{Cov}[\nabla_\phi W_\phi(x), J_\phi(x)] + \mathbb{E}[\nabla_\phi J_\phi(x)]. \end{aligned}$$

D.2. Exponential family and linear function

The gradient derived in the previous section can easily be applied to expectations with respect to functions linear in ϕ

under distributions in the exponential family. Let $J_\phi(x) = \xi_J(\phi)^T J(x)$ be a linear function in ϕ and suppose $W_\phi(x) = \xi_W(\phi)^T W(x)$ for some functions $\xi_J : \mathbb{R}^d \rightarrow \mathbb{R}^n$, $J : \mathcal{X} \rightarrow \mathbb{R}^n$ and $\xi_W : \mathbb{R}^d \rightarrow \mathbb{R}^m$, $W : \mathcal{X} \rightarrow \mathbb{R}^m$. Then

$$\begin{aligned} g_\phi(x) &= \text{Cov}[\nabla_\phi W_\phi(x), J_\phi(x)] + \mathbb{E}[\nabla_\phi J_\phi(x)] \\ &= \nabla_\phi \xi_W(\phi)^T \text{Cov}[W(x), J^T(x)] \xi_J(\phi) \\ &\quad + \nabla_\phi \xi_J(\phi)^T \mathbb{E}[J(x)] \end{aligned}$$

where $\nabla_\phi \xi(\phi)^T$ is the transposed Jacobian of ξ .

D.3. Symmetric KL: general case

Next we show that the symmetric KL divergence of Equation 13 can be rewritten as a sum of expectations over functions parametrized by ϕ , hence falling in the framework presented above.

For path parameter ϕ , the symmetric KL divergence is

$$\begin{aligned} \mathcal{L}_{\text{SKL}}(\phi) &= \sum_{n=0}^{N-1} \text{SKL}(\pi_{t_n}^\phi, \pi_{t_{n+1}}^\phi) \\ &= \mathbb{E} \left[\log \frac{\pi_{t_{n+1}}^\phi(X_{n+1})}{\pi_{t_n}^\phi(X_{n+1})} + \log \frac{\pi_{t_n}^\phi(X_n)}{\pi_{t_{n+1}}^\phi(X_n)} \right] \end{aligned}$$

where $X_n \sim \pi_{t_n}^\phi$. After cancellation of the normalization constants we obtain

$$\begin{aligned} \mathcal{L}_{\text{SKL}}(\phi) &= \sum_{n=0}^{N-1} \mathbb{E} [W_{t_{n+1}}^\phi(X_{n+1}) - W_{t_n}^\phi(X_{n+1}) \\ &\quad + W_{t_n}^\phi(X_n) - W_{t_{n+1}}^\phi(X_n)]. \end{aligned}$$

Collecting expectations under the same distribution and rearranging terms,

$$\begin{aligned} \mathcal{L}_{\text{SKL}}(\phi) &= \mathbb{E}[W_{t_0}^\phi(X_0) - W_{t_1}^\phi(X_0)] + \\ &\quad \sum_{n=1}^{N-1} \mathbb{E}[2W_{t_n}^\phi(X_n) - W_{t_{n+1}}^\phi(X_n) - W_{t_{n-1}}^\phi(X_n)] + \\ &\quad \mathbb{E}[W_{t_N}^\phi(X_N) - W_{t_{N-1}}^\phi(X_N)]. \end{aligned}$$

Defining for $n = 1, \dots, N-1$,

$$\begin{aligned} J_0^\phi(x) &= W_{t_0}^\phi(x) - W_{t_1}^\phi(x) \\ J_n^\phi(x) &= 2W_{t_n}^\phi(x) - W_{t_{n+1}}^\phi(x) - W_{t_{n-1}}^\phi(x) \\ J_N^\phi(x) &= W_{t_N}^\phi(x) - W_{t_{N-1}}^\phi(x), \end{aligned}$$

we have that

$$\mathcal{L}_{\text{SKL}}(\phi) = \sum_{n=0}^N \mathbb{E}[J_n^\phi(X_n)]$$

and

$$\nabla_{\phi} \mathcal{L}_{\text{SKL}}(\phi) = \sum_{n=0}^N \nabla_{\phi} \mathbb{E}[J_n^{\phi}(X_n)]$$

where $\nabla_{\phi} \mathbb{E}[J_n^{\phi}(X_n)]$ can be computed using the formula derived in Section D.1.

D.4. Symmetric KL: exponential family case

For the spline family introduced in Section 4, the distributions $\pi_{t_n}^{\phi}$ are in the exponential family with,

$$W_{t_n}^{\phi}(x) = \eta^{\phi}(t_n)^T W(x), \quad n = 0, \dots, N.$$

It follows that the functions J_n^{ϕ} are linear in ϕ with

$$\begin{aligned} J_0^{\phi}(x) &= z_0^{\phi T} W(x) \\ J_n^{\phi}(x) &= z_n^{\phi T} W(x), \quad n = 1, \dots, N-1 \\ J_N^{\phi}(x) &= z_N^{\phi T} W(x), \end{aligned}$$

where

$$\begin{aligned} z_0^{\phi} &= \eta^{\phi}(t_0) - \eta^{\phi}(t_1) \\ z_n^{\phi} &= 2\eta^{\phi}(t_n) - \eta^{\phi}(t_{n+1}) - \eta^{\phi}(t_{n-1}), \quad n = 1, \dots, N-1 \\ z_N^{\phi} &= \eta^{\phi}(t_N) - \eta^{\phi}(t_{N-1}). \end{aligned}$$

Given this relation, the stochastic gradient of Equation 13 can be evaluated using s samples from parallel tempering through the formula in Section D.2 defining:

$$\begin{aligned} X &= (X_0, \dots, X_N) \\ W(X) &= [W_0(X_0), W_1(X_0), \dots, W_0(X_N), W_1(X_N)]^T \\ J(X) &= W(X) \\ \xi_W(\phi) &= [\eta_0^{\phi}(t_0), \eta_1^{\phi}(t_0), \dots, \eta_0^{\phi}(t_N), \eta_1^{\phi}(t_N)]^T \\ \xi_J(\phi) &= [z_{0,0}^{\phi}, z_{0,1}^{\phi}, \dots, z_{N,0}^{\phi}, z_{N,1}^{\phi}]^T \end{aligned}$$

where X is the $s \times N$ matrix of samples from parallel tempering, $W(X)$ is a $s \times 2N$ matrix evaluating X elementwise at the reference and target distributions W_0 and W_1 , $\xi_W(\phi)$ is a $2N \times 1$ vector of annealing coefficients and $\xi_J(\phi)$ is a $2N \times 1$ vector of coefficients defining $J^{\phi} = [J_0^{\phi}, \dots, J_N^{\phi}]$.

E. Proof of proposition 2

For this annealing path family,

$$W_t(x) = \eta(t)^T W(x).$$

where η is parametrized so that $\|\eta'(t)\|_2 = L$. Therefore, the piecewise twice continuous differentiability of $\eta(t)$ and

endpoint conditions imply that conditions 1 and 2 of Definition 1 are satisfied. Next, note that

$$\begin{aligned} \left| \frac{dW_t}{dt} \right| &= |\eta'(t)^T W(x)| \leq L \|W(x)\|_2 \\ \left| \frac{d^2 W_t}{dt^2} \right| &= |\eta''(t)^T W(x)| \leq M \|W(x)\|_2, \end{aligned}$$

and thus we set $V_1(x) = V_2(x) = (L+M)\|W(x)\|_2$. Since $\eta([0, 1]) \subseteq \Omega$, and noting that $\mathbb{E}[\|W(X)\|_2^3] < \infty$ implies $\mathbb{E}[\|W(X)\|_2] < \infty$ by Jensen's inequality, the path satisfies condition 3 of Definition 1. Finally, note that Ω is a convex subset of \mathbb{R}^2 : for any nonnegative function $G(x)$, vectors $\xi_1, \xi_2 \in \mathbb{R}^2$, and $\lambda \in [0, 1]$,

$$\begin{aligned} &\exp((\lambda \xi_1 + (1-\lambda)\xi_2)^T W(x)) G(x) \\ &= (\exp(\xi_1^T W) G(x))^{\lambda} (\exp(\xi_2^T W) G(x))^{1-\lambda} \end{aligned}$$

and so Hölder's inequality $\int f^{\lambda} g^{1-\lambda} \leq (\int f)^{\lambda} (\int g)^{1-\lambda}$ yields log-convexity (and hence convexity). Therefore as long as the endpoints $(0, 1)$ and $(1, 0)$ are in Ω —which is the case if the family is nonempty—any convex combination of $(0, 1)$ and $(1, 0)$ is also in Ω and therefore the linear path is included.

F. Empirical support for the SKL surrogate objective function

Two objective functions were discussed in Section 3: one based on rejection rate statistics, i.e. Equation (10), and the symmetric KL divergence (SKL). In this section we perform controlled experiments comparing the signal-to-noise ratio of Monte Carlo estimators of the gradient of these two objectives. Let G denote a Monte Carlo estimator of a partial derivative with respect to one of the parameters ϕ_i . Refer to D for details on the stochastic gradient estimators. In this experiment we use i.i.d. samples so that the Monte Carlo estimators are unbiased, justifying the use of the variance as a notion of noise. Hence following (Rainforth et al., 2018), we define the signal-to-noise ratio by $\text{SNR} = |\mathbb{E}[G]|/\sigma[G]$, where $\sigma[G]$ denotes the standard deviation of G . We use two chains with one set to a standard Gaussian, the other to a Gaussian with mean ϕ and unit variance. We show the value of the two objective functions in Figure 4 (left). The label ‘‘Rejection’’ refers to the expected rejection of the swap proposal between the two chains, r . We also show the square root of half of the SKL (‘‘SqrtHalfSKL’’), to quantify the tightness of the bound in Equation (13), while ‘‘Ineff’’ shows the rejection odds, $r/(1-r)$, called inefficiency in (Syed et al., 2019).

Signal-to-noise ratio estimates were computed for each parameter $\phi_i \in \{0, 1/5, 2/5, \dots, 2\}$. Each gradient estimate uses 50 samples, and to approximate the signal-to-noise ratio the estimation was repeated 1000 times for each ϕ_i and

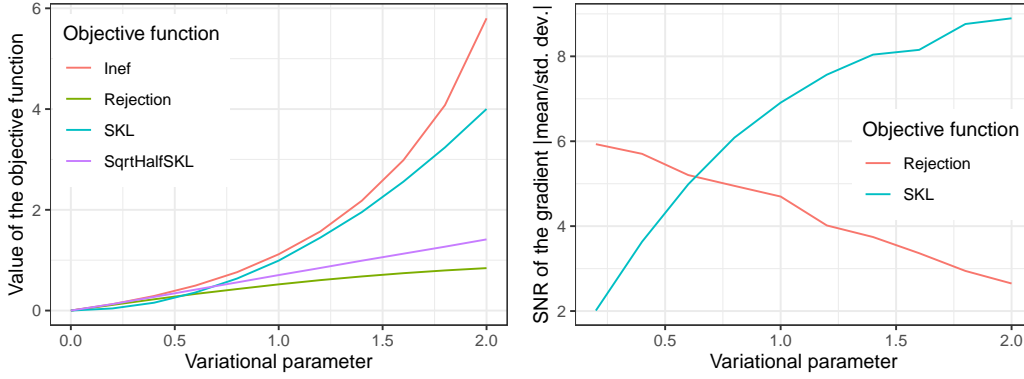


Figure 4. Left: objective functions for path optimization in a controlled experiment as a function of a variational parameter ϕ . Right: signal-to-noise of corresponding gradient estimators on the same range of parameters.

objective function. The results are shown in Figure 4 (right), and show that in the regime of small rejection ($< \approx 30\%$), the gradient estimator based on the rejection objective has a superior signal-to-noise ratio compared to its SKL counterpart. However as ϕ increases and the two distributions become farther apart, the situation is reversed, providing empirical support for the surrogate objective for challenging path optimization problems.

G. Experimental details

All the experiments were conducted comparing reversible PT, non-reversible PT and non-reversible PT based on the spline family with $K \in \{2, 3, 4, 5, 10\}$.

Every method was initialized at the linear path with equally spaced schedule, i.e. $\pi_t \propto \pi_0^{1-t/N} \pi_1^{t/N}$ with N the number of parallel chains. All methods performed one local exploration step before a communication step.

To ensure a fair comparison of the different algorithms, we fixed the computational budget to a pre-determined number of samples in each experiment. Reversible PT used the budget to perform local exploration steps followed by communication steps. In non-reversible PT the computational budget was used to tune the schedule according to the procedure described in (Syed et al., 2019, Section 5.1). For non-reversible PT with path optimization, the computational budget was divided equally over a fixed number of scans of Algorithm 2, where a scan corresponds to one iteration of the for loop.

Optimization of the spline annealing path family was performed using the SKL surrogate objective of Equation 13. Adagrad was used for the optimization. The gradient was scaled elementwise by its absolute value plus the value of the knot component. Such scaling was necessary to limit the gradient in the interval $[-1, 1]$, stabilizing the optimization and avoiding possible exploding gradients due to the

transformation to log space.

To mitigate variance in the results due to randomness, we performed 10 runs of each method and averaged the results across the runs.

G.1. Gaussian

This experiment optimized the path between the reference $\pi_0 = N(-1, 0.01^2)$ and the target $\pi_1 = N(1, 0.01^2)$. We used $N = 50$ parallel chains initialized at a state sampled from a standard Normal distribution. In this setting, π_t has a closed form that can be shown to be $N\left(\frac{\eta_1(t) - \eta_0(t)}{\eta_0(t) + \eta_1(t)}, \left(\frac{0.01^2}{\eta_0(t) + \eta_1(t)}\right)^2\right)$, therefore, in the local exploration step of parallel tempering we sampled i.i.d. from π_t . The computational budget was fixed at 45000 samples. Non-reversible PT with optimized path divided the budget in 150 scans. Therefore, for every gradient step in Algorithm 2, the gradient was estimated with 300 samples. We used 0.2 as learning rate for Adagrad.

G.2. Beta-binomial model

The second experiment was performed on a conjugate Bayesian model. The model prior was $\pi_0(p) = \text{Beta}(180, 840)$. The likelihood was $L(x|p) = \text{Binomial}(x|n, p)$. We simulated $x_1, \dots, x_{2000} \sim \text{Binomial}(100, 0.7)$, resulting in a posterior distribution $\pi_1(p) = \text{Beta}(140180, 60840)$. The prior is concentrated at 0.176 with a standard deviation of 0.0119. The posterior distribution is concentrated at 0.697 with a standard deviation of 0.001. We used $N = 50$ parallel chains initialized at 0.5. Also in this experiment it is possible to compute π_t in closed form. Let $S = \sum_{i=1}^{2000} x_i$, $R = 2000 \times 100$ then $\pi_t(p) = \text{Beta}(179\eta_0(t) + (180 + S - 1)\eta_1(t) + 1, 839\eta_0(t) + (840 + N - S - 1)\eta_1(t) + 1)$. Hence, in the local exploration step of parallel tempering we sampled i.i.d. from π_t . The

computational budget was fixed at 45000 samples. Non-reversible PT with optimized path divided the budget in 150 scans. Therefore, for every gradient step in Algorithm 2, the gradient was estimated with 300 samples. We used 0.2 as learning rate for Adagrad.

G.3. Mixture model

The third experiment was a Bayesian Gaussian mixture model with mixture proportions w_0, w_1 , mixture component densities $N(\mu_i, 10^2)$ for mean parameters μ_0, μ_1 , and a binary cluster label for each data point. We placed a $\text{Dir}(1, 1)$ prior on the proportions, and a $N(150, 1)$ prior on each of the two mean parameters. We simulated $n = 1000$ data points from the mixture $0.3N(100, 10^2) + 0.7N(200, 10^2)$. We used $N = 35$ chains. Mixture proportions were initialized at 0.5, mean parameters were initialized at 0 and cluster labels were initialized at 0. The local exploration step involved standard Gibbs steps for the means, indicators, and proportions. To improve local mixing, we also included an additional Metropolis-Hastings step for the proportions that approximates a Gibbs step when the indicators are marginalized. The computational budget was fixed at 25000 samples. Non-reversible PT with optimized path divided the budget in 50 scans. Therefore, for every gradient step in Algorithm 2, the gradient was estimated with 500 samples. We used 0.3 as learning rate for Adagrad.